Gas-Solid Catalytic Reactions with an Extended DSMC Model

Georg R. Pesch
Foundation Institute of Materials Science (IWT), Dept. of Production Engineering, University of Bremen, Germany

Chemical Engineering—Recovery and Recycling (VdW), Dept. of Production Engineering and Center for Environmental Research and Sustainable Technology (UFT), University of Bremen, Germany

Norbert Riefler and Udo Fritsching
Foundation Institute of Materials Science (IWT), Dept. of Production Engineering, University of Bremen, Germany

Lucio Colombi Ciacchi
Hybrid Materials Interfaces Group (HMI), Dept. of Production Engineering and Bremen Center for Computational Materials Science (BCCMS), University of Bremen, Germany

Chemical Engineering—Recovery and Recycling (VdW), Dept. of Production Engineering and Center for Environmental Research and Sustainable Technology (UFT), University of Bremen, Germany

Lutz Mädler
Foundation Institute of Materials Science (IWT), Dept. of Production Engineering, University of Bremen, Germany

DOI 10.1002/aic.14856
Published online May 13, 2015 in Wiley Online Library (wileyonlinelibrary.com)

An algorithm of diffusive gas transport in porous solids based on random collisions of molecules (DSMC) is extended to include basic heterogeneous reaction mechanisms (adsorption, coadsorption, desorption, and reaction of gas species on the surface of the solid). With this model, we study the catalytic oxidation of CO inside highly porous nanoparticle layers in the transition regime using kinetic parameters from Pd(111) surfaces at ultra high vacuum conditions. Investigation of the reaction at different temperatures reveals a clear transition between a kinetic limit (low temperatures) and a diffusion limit (high temperatures). At high temperatures and under steady-state conditions, the porous layer shows three distinct regions with different reaction rates (reactor poisoning, an effective reaction region, and a region with CO depletion), whose extends are determined by CO concentration and mass-transport limitation. We expect that similar investigations help optimizing the structure of gas sensor elements based on nanoparticle layers fabricated with flame spray pyrolysis. © 2015 American Institute of Chemical Engineers *AIChE J*, 61: 2092–2103, 2015
Keywords: heterogeneous catalytic reaction, gas diffusion, direct simulation Monte Carlo, high porosity, gas sensor

Introduction

Heterogeneous catalytic processes involve various time and length scales. Adsorption and reaction processes occur within femtoseconds to picoseconds on a lengthscale of nanometers (microscale); diffusive transport of molecules takes place within nanoseconds or microseconds over several micrometers (mesoscale); and the convective exchange of substances requires milliseconds or longer over several millimeters or more (macroscale). Therefore, designing heterogeneous catalytic processes requires multiscale models. A detailed simultaneous modeling of all these processes is beyond the current simulation capabilities,[1] but combining established models to bridge the different scales is a viable approach.[2]

Density functional theory (DFT)[3] is an *ab initio* method to compute interatomic forces from quantum-mechanical ground-state electron densities. The method can be used to find energetically favored reaction configurations but is limited to simulation times of the order of 10 ps for systems of a few hundred atoms. Classical interaction potentials (force fields) are used in molecular dynamics (MD) simulations for the modeling of transport in gases on and to surfaces over time spans of up to a microsecond on a 100 nm length scale. Larger time scales up to seconds can be reached with the kinetic Monte Carlo (kMC) method.[4] This method requires rates of atomic/molecular processes as input parameters in order to capture surface reactions. However, neither MD nor kMC methods are suitable to resolve transport that involves a transition from the continuum to the free molecular regime, for example, within a gas-filled porous structure. Here, methods such as the dusty gas model (DGM)[5] are commonly applied in order to describe transport processes with reactions. DGM uses specific source terms describing adsorption, desorption and reaction rates as a coupled partial differential equation system. In DGM models, the effect of the pore structure on the transport properties is expressed with the help of averaged

Correspondence concerning this article should be addressed to L. Mädler at lmaedler@iwt.uni-bremen.de.

parameters such as porosity and tortuosity. At the macroscale, computational fluid dynamics (CFD) tools are widely used to model mass and heat transfer.

In some cases these methods already bridge different scales. For instance, the DGM can be coupled with CFD[6] by implementing a specific source term in a commercial CFD software to describe reaction and diffusion processes within a porous layer embedded in a convective fluid flow with heat transfer. Votsmeier[7] described a modification of commercial CFD software in which complex microkinetic models are replaced by chemical source terms from precomputed surface chemistry data. However, these methods often suffer from the loss of local information. For smaller length scales, DFT-based kMC simulations connect molecular with mesoscopic processes[8,9] considering concurrent adsorption, desorption, and chemical reaction at the catalytic surface. However, a coupling with the surrounding gas is difficult to implement. A promising method connecting simulations on different length scales is the Direct Simulation Monte Carlo (DSMC) method[10] which is based on the Monte Carlo (MC) concept of randomization of molecular interactions. This method statistically simulates realistic transport processes on the meso and macro scales. An extension of the DSMC method which takes into account chemical reactions has been described by Bird.[11] However, the chemical reactions are limited to molecular collisions in the gas phase, whereas surface reactions have not been considered yet.

This article describes an extension of the DSMC method to consider adsorption, desorption, coadsorption, and reaction of molecules on surfaces. A model is presented that effectively combines molecular interactions and transport processes without the loss of detailed structural information on different length scales. We have extended the DSMC method which has been implemented into the OpenFOAM CFD software package by Scanlon et al.[12] and modified by Dreyer et al.[13] to correctly simulate diffusion processes. In our implementation, the model covers a length scale of the order of 1 μm, with a resolution of the order of 1 nm.

With our newly developed method, we are able to investigate the diffusion and reaction processes inside active gas sensor elements fabricated with an aerosol synthesis method (flame spray pyrolysis, FSP). In such systems,[14–16] two interdigitated electrodes are covered with a porous nanoparticle (NP) layer. When a gas with unknown composition diffuses into these layers, it adsorbs on the NP surfaces and subsequently reacts. The reactions cause a resistivity change in the layer, which is measured by the electrodes and can be used to determine the gas composition through an adequate calibration.

Fundamental for the structural design and the response optimization of gas sensors of this kind is precise knowledge about the amount of reacting gas and the location of the reaction fronts within the layer. For this specific case, established models are not able to map the precise processes on the surface in combination with gas diffusion, as they are always approximating either for the surface chemical processes or for the gas diffusion. In this work, we model the diffusion and oxidation reaction of CO molecules over an anisotropic porous layer of palladium NPs with geometries which resemble typical highly porous FSP NP layers.[14,17] These layers are characterized by high specific surface area and fast gas diffusion rates, as already verified by means of DSMC with the variable soft sphere (VSS) model.[13] The simulation parameters for adsorption, desorption, and reaction are obtained from experimental studies of CO oxidation over single-crystal Pd(111) surfaces under ultra high vacuum (UHV) conditions,[18] a system which have been very thoroughly investigated and is therefore ideal for the purposes of testing our simulation method. All simulations presented here are conducted at atmospheric pressure, in order to keep the simulation time within reasonable limits. We are aware that the UHV reaction conditions are not simply transferable to atmospheric pressure,[19] so that some of the simulation parameters are not representative of the experimental reality (for instance, Pd NPs become fully oxidized at high temperatures and atmospheric oxygen pressure). Therefore, our results are to be considered only as a fundamental proof of our algorithms and their numerical implementations, applied to a simple and well-know reaction mechanism.

Theoretical Approach and Validation

Catalytic reaction mechanism

Many heterogeneous reactions, for example, CO oxidation on Pd(111), proceed according to the Langmuir-Hinshelwood (LH) mechanism, in which both reactants need to adsorb on the catalysts surface before chemical reactions occur.[20] In cases where different partial reaction steps are considered, the reaction mechanism is described with a set of equations requiring rate constants for the forward and reverse reactions of each individual step. Equations 1a–1d show the partial steps involved in the overall CO oxidation reaction, $CO + O_2 \rightarrow CO_2$

$$CO + * \underset{k_2}{\overset{k_1}{\rightleftharpoons}} CO_{ads}, \tag{1b}$$

$$O_2 + 2* \underset{k_4}{\overset{k_3}{\rightleftharpoons}} 2O_{ads}, \tag{1b}$$

$$O_{ads} + CO_{ads} \xrightarrow{k_5} CO_{2,ads}, \tag{1c}$$

$$CO_{2,ads} \xrightarrow{k_6} CO_2 + *. \tag{1d}$$

Here, * denotes an unoccupied surface site. The reaction rates k_1 and k_3 denote the adsorption of CO and O_2, respectively, whereas k_2 and k_4 denote their desorption. In most cases CO adsorbs molecularly, while a possible dissociative adsorption does not contribute to the formation of CO_2.[18] Oxygen adsorbs at temperatures above 150–200 K dissociatively onto the Pd(111) surface[21] and therefore molecular O_2 adsorption is not considered. The LH step in which both reactants form the product proceeds irreversibly with the rate constant k_5. After the reaction, the chemisorbed CO_2 desorbs instantaneously, so $k_6 \rightarrow \infty$ in Eq. 1d.

Simulation algorithm

The basis of our simulation algorithm is the DSMC method,[10] which has been implemented in the open source software package OpenFOAM by Scanlon et al.,[12] and recently expanded with the VSS method by Dreyer et al.[13] The application of MC simulation methods are based on reliable random number generators with a high amount of randomness.[10,22] Convenient random number generators deliver uniformly distributed numbers in the range of $0 \leq R_f \leq 1$.

A sketch of the modified DSMC algorithm is shown in Figure 1. Three main steps are conducted during each simulation time step. The first two, that is, particle movement and collision sampling, are taken from the original DSMC algorithm with slight modifications. These two steps are described and discussed in detail elsewhere.[10,13] Briefly, in the first step the

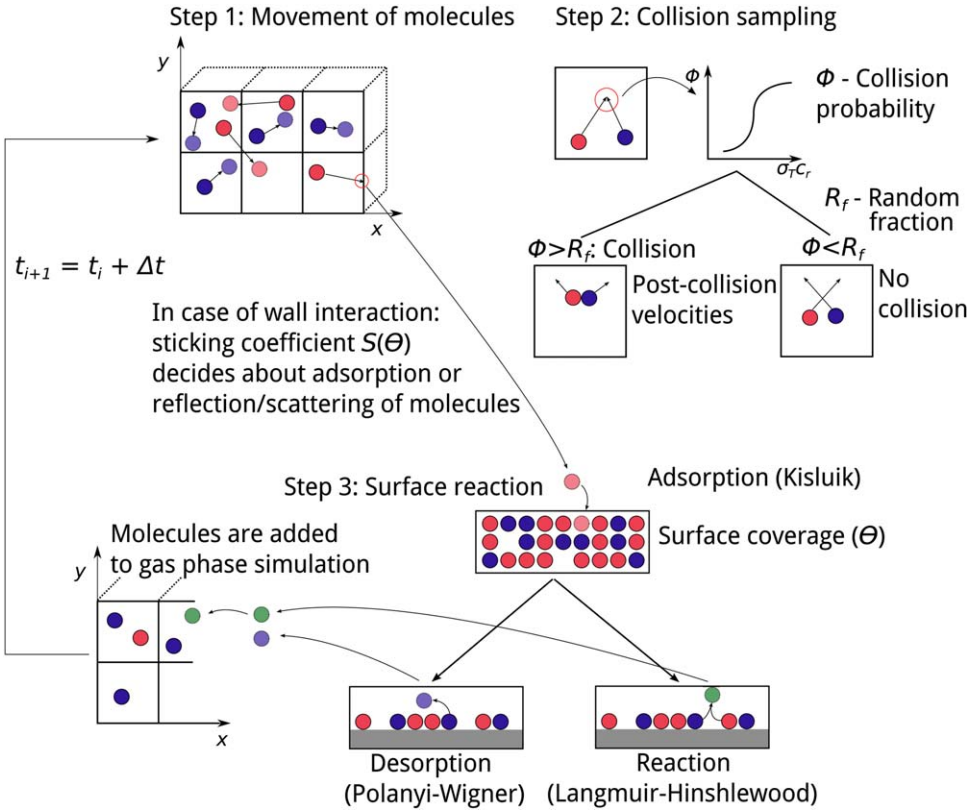

Figure 1. Sketch of the modified the DSMC algorithm. Three main steps are conducted during each simulation time step.

Step 1: molecules in the simulation volume are moved according to their velocities. Step 2: collisions of the molecules with each other are simulated. If a molecule hits a wall in the first step, this may lead to adsorption. Step 3: two processes are conducted in parallel. Based on the current surface coverage the amount of desorbing and reacting molecules is calculated based on the Polanyi-Wigner equation (Eq. 8) and on an Arrhenius type equation based on the LH mechanism (Eq. 14), respectively. With step 3 the cycle is closed and the algorithm starts again at step 1 with the time being advanced by $t_{i+1} = t_i + \Delta t$. [Color figure can be viewed in the online issue, which is available at wileyonlinelibrary.com.]

molecules are moved according to their velocities and a new position vector is identified ($u = s/t$). The second step comprises the sampling of collisions between molecules, where each pair of molecules from the same cell has an assigned collision probability Φ according to the collision cross section σ_T and the relative velocity c_r between the two molecules. The collision probability is then compared with a random number. If collision occurs, post-collision velocity vectors are assigned to the selected molecules.[10]

For a correct expression of the gas phase diffusion processes, the collisions between two molecules including scattering angles and post-collision velocities have to be modeled. Here, we use the VSS model[13] with parameters taken from Bird.[10] Table 1 lists parameters for O_2, CO, and CO_2, respectively. Table 2 lists scattering parameters for the calculation of scattering angles after collisions between unlike molecules. In case of collisions between two molecules of the same kind, α_{12} takes the value α from Table 1.

If a molecule hits a wall, adsorption might occur according to the adsorption algorithm described in the following section.

In the third step, either molecular desorption or chemical reaction takes place. The desorption rate is calculated for each species (O and CO) based on their current surface densities σ_{CO} and σ_O, respectively. The amount of generated CO_2 molecules due to reaction is calculated using an Arrhenius type equation based on the LH reaction mechanism (see section Reaction mechanism). The amount of generated molecules from all three species after the reaction and desorption steps is then added to the gas phase cells and considered in subsequent diffusion processes in the next time step. The surface chemical processes, as well as the applied parameters and their physical origin, are described in the following sections.

Table 1. Molecule Parameters of O_2, CO, and CO_2 for the DSMC Simulation Using the VSS Model[10] at $T = 273$ K and $p = 101.3$ kPa

Parameter	Mass of Molecule	Viscosity Index	Viscosity	Scattering Parameter	Degrees of Freedom
Symbol	m	ω	μ	α	f
Unit	kg	–	Nm s^{-1}	–	–
O_2	5.31×10^{-26}	0.77	1.919×10^{-5}	1.40	5
CO	4.65×10^{-26}	0.73	1.635×10^{-5}	1.49	5
CO_2	7.31×10^{-26}	0.93	1.380×10^{-5}	1.61	6.7

Table 2. VSS Scattering Parameter α_{12} for Collisions Between Unlike Molecules[10]

Molecule Pair	α_{12}
CO–CO_2	1.61
CO–O_2	1.54
O_2–CO_2	1.72

Adsorption mechanism

As soon as a molecule hits a surface during the gas phase simulation step, an adsorption probability is calculated based on the sticking coefficient S. The sticking coefficient is the ratio of adsorbing molecules, N_{ads}, and incident molecules, N_{inc}, on a given surface, $S = N_{ads}/N_{inc}$, and depends on the surface coverage θ of already adsorbed molecules. The surface coverage of a molecular species θ is defined as the ratio σ/σ_N between the number of adsorbed molecules on a given surface area, σ, and the number of surface atoms, σ_N. At every step in our simulations, for each considered molecule, the sticking coefficient S is compared with a random number $R_f \in [0, 1]$ in order to decide if adsorption of a molecule occurs. The considered molecule adsorbs and is thus deleted from the gas phase simulation if $S > R_f$. Instead, if $S < R_f$, the molecule is scattered away from the surface with a velocity vector sampled from the Maxwell-Boltzmann distribution according to the surface temperature.

Among the several models available to calculate the sticking coefficient,[20,23] we use the precursor-mediated adsorption model introduced by Kisluik[24,25]

$$S(\theta) = S_0\left(1+K\left(\frac{1}{\theta_{req}}-1\right)\right)^{-1}. \tag{2}$$

Here, $S_0 \leq 1$ is the initial sticking coefficient for a surface with a coverage $\theta = 0$ for that molecule species, and θ_{req} is the probability to find the required number of adjacent empty sites on the surface[20]

$$\theta_{req} = \left(1-\frac{\theta}{\theta_{max}}\right)^{n}, \tag{3}$$

with the adsorption order $n = 1$ describing molecular (CO) and $n = 2$ dissociative (O_2) adsorption and θ_{max} being the coverage of a fully saturated surface. The prefactor K is defined as

$$K = \frac{f'_{des}}{f_{ads}+f_{des}}, \tag{4}$$

where f'_{des} is the probability of a molecule to desorb from the precursor state over an occupied site into the gas phase, whereas f_{ads} and f_{des} are the probabilities of molecules which are in a precursor state over an unoccupied site to adsorb onto the surface or to desorb into the gas phase, respectively. The initial sticking coefficient in turn depends on the probability γ of a molecule to enter into the precursor state

$$S_0 = \gamma\left(1+\frac{f_{des}}{f_{ads}}\right)^{-1}. \tag{5}$$

Lateral interactions between unlike molecules can lead to rather complex coadsorption mechanisms as it is the case for O_2 and CO on Pd(111). The full mechanism has been described in detail by Engel and Ertl.[18] Briefly, gaseous O_2 adsorbs dissociatively on Pd(111) until a saturation coverage of $\theta_{max} = 0.25$ is reached. At high pressures, O_2 reacts with the surface atoms to form surface oxides, PdO_x, which may have a higher reactivity toward CO oxidation.[19,26] Carbon monoxide adsorbs molecularly on the Pd(111) surfaces, with a maximum surface coverage of $\theta_{max} = 0.5$ at room temperature. If CO adsorbs first, it inhibits O_2 adsorption. At coverages $\theta_{CO} < 1/3$, O_2 can still adsorb and both species are either scattered randomly on the surface in case of low coverages or form separated domains in case of moderate and high coverages. In latter case, the reaction takes place at the domain boundaries, changing the reaction order of the LH step from 2 to 1. For $\theta_{CO} > 1/3$, O_2 adsorption is completely inhibited. If O_2 adsorbs first, CO is able to adsorb even on surfaces with $\theta_O = \theta_{O,max}$ and is thus compressing the O_{ads} in domains with higher local coverage. The compression of the O_{ads} increases with CO coverage until both structures finally form a mixed domain with local coverages $\theta_{CO} = \theta_O = 0.5$. Increasing compression of either CO or O domains is always linked to a decrease in binding energy of both species and thus lower desorption and reaction activation energies. A more detailed description is given in Refs. 18, 23 and references therein. The surface coverages of CO and O are connected to the pressure and the partial pressure ratio of CO and O_2 through adsorption equilibrium constants.[23]

In the present implementation, the lateral interactions between like or unlike molecules described above are taken into account by modifying Eq. 3 so that O_2 adsorption is hindered by adsorbed CO, whereas CO adsorption is not hindered by adsorbed O[20]

$$\theta_{req,CO} = \frac{\theta_{max,CO}-\theta_{CO}}{\theta_{max,CO}}, \tag{6a}$$

$$\theta_{req,O} = \left(1-\frac{\theta_O}{\theta_{max,O}}-\frac{\theta_{CO}}{\theta_{max,CO}}\right)^{2}. \tag{6b}$$

The coverages θ and θ_{max} are expressed according to the lengths of the surface unit cell vectors **a** and **b**, which for a fcc(111) crystal obey the relationship

$$|\mathbf{a}| = |\mathbf{b}| = \frac{\sqrt{2}}{2}a_0, \tag{7}$$

with a_0 being the lattice constant. The amount of adsorption sites N_0 for a given surface area A is calculated as $N_0 = A/|\mathbf{a}|^2$. The parameter $\theta_{max} = N_{ads,max}/N_0$ is obtained from the literature. Namely, for CO $\theta_{max} = 1/3$ is selected because it represents the maximum value at ambient temperature at which oxygen adsorption is still possible.[27] For O, we set $\theta_{max} = 0.25$ in accordance with Refs. 28–30.

The adsorption parameters K and S_0 are fitted to experimental data for each adsorbing species. The obtained values $S_0 = 1$ and $K = 0.60$ for CO are independent on the temperature and are determined by fitting the Kisluik model to the experimental $S(\theta)$ curves presented in Ref. 27. The sticking coefficient of O_2 is temperature dependent, and experimental $S(\theta)$ curves are reported in Ref. 30 for four different temperatures. The corresponding Kisluik parameters for temperatures from 323 to 823 K are obtained by fits to these four curves (Figure 2). Values between the four temperatures and above have been obtained by linear interpolation and extrapolation, respectively (Table 3).

Desorption mechanism

The kinetics of desorption are described by the Polanyi-Wigner equation[20]

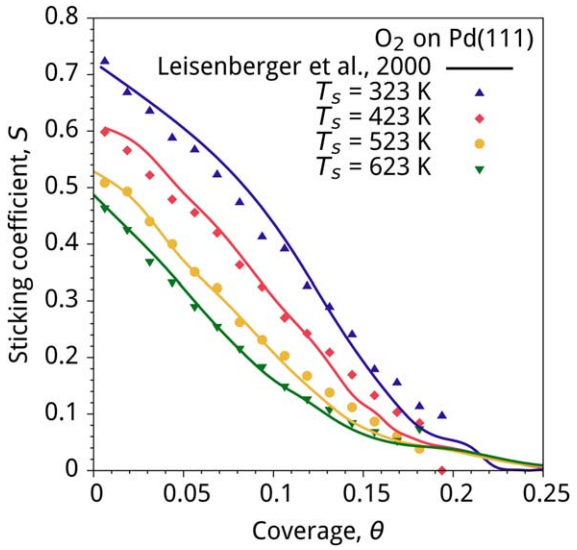

Figure 2. Sticking coefficient S of O_2 dissociatively adsorbing on a Pd(111) surface for different coverages θ, different surface temperatures T_s and constant gas temperature $T_g = 300$ K.

Symbols denote data obtained from the modified DSMC simulation. Adsorption parameters are extracted from fitting to the experimental results by Leisenberger et al.,[30] which are plotted for comparison (lines). [Color figure can be viewed in the online issue, which is available at wileyonlinelibrary.com.]

$$r_{\mathrm{des}} = -\frac{\partial\theta}{\partial t} = \nu_{\mathrm{des}}\theta^n \exp\left(\frac{-E_{\mathrm{des}}}{RT}\right), \tag{8}$$

which relates the desorption rate r_{des} to the activation energy E_{des}, the pre-exponential factor ν_{des} and the surface temperature T. The desorption order is $n = 1$ for molecular CO desorption and $n = 2$ for associative O_2 desorption. The activation energy depend linearly on the coverage θ

$$E_{\mathrm{des}}(\theta) = E_{\mathrm{des}}(0) + W\theta, \tag{9}$$

with the energy of molecular interaction W describing the weakening ($W < 0$) or intensification ($W > 0$) of adsorption bonds due to lateral interactions between adsorbed molecules. W is defined via the number of nearest neighbors at a fully saturated surface, N_{nn}, and their interaction potential, ω_{pair}, so that $W \times \theta_{\mathrm{max}} = \omega_{\mathrm{pair}} \times N_{\mathrm{nn}}$.

Values for E_{des} and ν_{des} can be measured using temperature-programmed desorption (TPD) and evaluated, for example, using the Redhead analysis[20]

$$E_{\mathrm{des}} = RT_{\mathrm{p}}\left(\ln\left(\frac{\nu T_p}{\beta}\right) - 3.46\right), \tag{10}$$

where T_{p} is the temperature at the desorption maximum and β the temperature ramping slope. More detailed analyses for the variation of E_{des} and ν_{des} with θ are described in Ref. 31. Often, $E_{\mathrm{des}}(\theta)$ and $\nu_{\mathrm{des}}(\theta)$ vary in concert as expressed with the compensation effect

$$\ln\nu_{\mathrm{des}}(\theta) = \frac{E_{\mathrm{des}}(\theta)}{RT_c} + c, \tag{11}$$

where c is a constant and T_c is the isokinetic temperature. The compensation effect does not necessarily apply for all reaction systems. However, the pre-exponential may nevertheless change over several orders of magnitude with coverage, which we express in our algorithm implementation using the power law relation

$$\nu_{\mathrm{des}} = 10^{C_a + C_b\theta}. \tag{12}$$

In this equation both constants C_a and C_b are fitting parameters, which do not represent any physical quantities, but are solely introduced in order to be able to fit experimental $\nu_{\mathrm{des}}(\theta)$ curves.

In our simulations, a loop iterates through all surface sites for every adsorbed species (CO_{ads} and O_{ads}) and calculates the respective desorption rates. The chance of desorption for a single molecule in a given timestep Δt is calculated according to

$$P_{\mathrm{des}} = \frac{r_{\mathrm{des}}\Delta t}{\sigma}, \tag{13}$$

where $\sigma = N_{\mathrm{ads}}/N$ is the surface density of the considered species. A molecule desorbs if $P_{\mathrm{des}} > R_f$. If desorption takes place, r_{des} and Eq. 13 are recalculated with the new coverage for all adsorbed molecules until no desorption events occur within the same timestep.

The characteristic parameters for desorption, E_{des} and ν_{des}, and their change with coverage are obtained by analyzing TPD spectra as reported in Ref. 21 for O_2 and Ref. 32 for CO, under the assumption that the Polanyi-Wigner equation is valid (Table 4). Figure 3 shows the TPD plots of oxygen desorbing from a Pd(111) surface calculated with an applied temperature ramping slope $\beta = 2$ K s^{-1}, over an effective desorption area $A = 2\times10^{-10}$ cm^2 and using a time step $\Delta t = 0.1$ s. Best fits to the experimental single-crystal results of Guo et al.[21] (solid lines) are obtained for a pairwise nearest-neighbor interaction energy between adsorbed O_{ads} atoms of 2.9 kJ mol^{-1}, which agrees well with Ref. 21. The fact that O_{ads} has 6 nearest neighbors at maximum coverage $\theta_{\mathrm{max}} = 0.25$ results in $W = -69.6$ kJ mol^{-1}. The temperature at maximum oxygen desorption decreases with increasing initial coverage from 820 K ($\theta_0 = 0.08$) to 780 K ($\theta_0 = 0.16$), due to lateral interactions. The overall desorption rate of O_2 molecules is negligible for $T < 700$ K, whereas for higher temperatures oxygen desorbs, considerably shifting the adsorption–desorption equilibrium.

Table 3. O_2 Adsorption Parameters, Interpolated with Values from Figure 2.

Temperature, T_s	K	S_0
323 K	0.45	0.72
423 K	0.60	0.62
473 K	0.71	0.60
523 K	0.82	0.56
573 K	0.95	0.52
623 K	1.11	0.49
673 K	1.29	0.45
723 K	1.49	0.42
773 K	1.71	0.38
823 K	1.97	0.34

Table 4. O_2 and CO Desorption Parameters for the Polanyi-Wigner Equation[21,32]

Parameter	$E_{\mathrm{des},0}$	W	$C_a(\nu_{\mathrm{des}})$	$C_b(\nu_{\mathrm{des}})$
Unit	kJ mol^{-1}	kJ mol^{-1}	–	–
O_2	222	−69.6	−17	0
CO	147	−153	16	−15

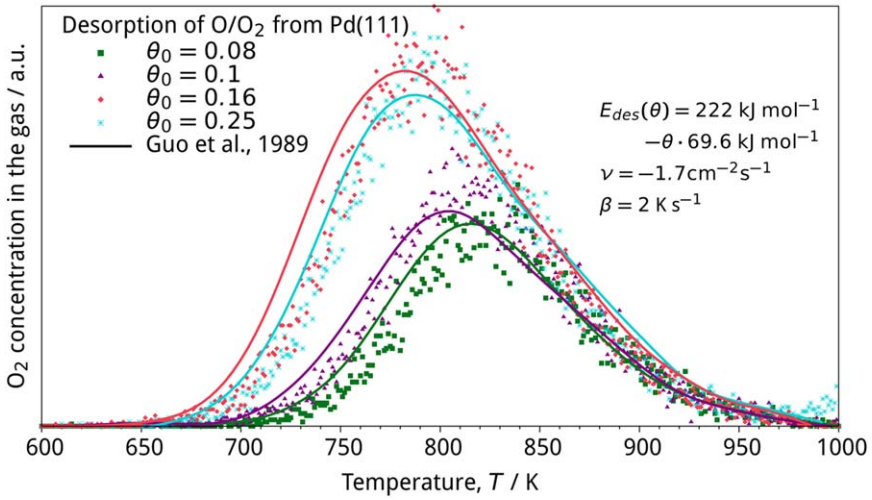

Figure 3. Desorption of O_2 from a Pd(111) surface in a simulated TPD experiment with different initial surface coverages θ_0.

The applied temperature slope was $\beta = 2$ K s^{-1}. The symbols denote simulated results, obtained with DSMC. Shown is the amount of desorbing molecules in intervals of 0.1 s. Experimental results from Guo et al.[21] are shown for comparison, scaled by an arbitrary multiplicative factor to match the simulated peak intensities. [Color figure can be viewed in the online issue, which is available at wileyonlinelibrary.com.]

Reaction mechanism

The rate of CO_2 formation, r_{CO_2}, is described with the Arrhenius equation

$$r_{CO_2} = \nu_{LH} f(\sigma_{CO}, \sigma_O) \exp\left(-\frac{E_{LH}}{RT}\right), \tag{14}$$

which includes the pre-exponential of the reaction ν_{LH}, a function $f(\sigma_{CO}, \sigma_O)$ taking into account the dependence of the reaction rate on the surface coverages, the activation energy E_{LH} and the temperature T. Both E_{LH} and ν_{LH} strongly depend on the coverage of both species and their respective adsorption order. The assumption of a second order reaction process, $f(\sigma_{CO}, \sigma_O) = \sigma_{CO}\sigma_O$, is valid if both coverages are low and both species are scattered randomly on the surface, which is what we assume for this work. We note that if surface domains are present, f provides a value for the effective intersection length between O and CO domains and the reaction process become first order, since the reaction is only pursued at the domain boundaries.

The pre-exponential factor and activation energy of the surface reaction step are system-specific. Intrinsic reaction barriers from the literature[33] are used to calculate the reaction kinetics of our model system ($E_{LH} = 84$ kJ mol^{-1} and $\nu_{LH} = 2.5 \cdot 10^{-3}$ cm^2 s^{-1}). The reaction probability r_{CO_2} is calculated following Eq. 13 as $P_{CO_2} = r_{CO_2} \cdot \Delta t/\sigma$, and compared with a random number. Desorption of a reacted molecule occurs instantly, with the position and velocity vector of the generated molecule calculated according to the desorption algorithm described above.

Coadsorption behavior is implemented according to the following model: Oxygen adsorption is actively inhibited by CO_{ads} with no possibility for O_2 to adsorb on a surface when $\theta_{CO} = \theta_{CO,max}$ (cf. Eq. 6a), while CO adsorption is not inhibited by adsorbed O_{ads} species (the sticking coefficient of CO is not influenced by O_{ads}). Therefore, the model accounts for catalyst poisoning. Even if a surface is preadsorbed by oxygen, CO is still able to adsorb and, as soon as an oxygen molecule desorbs, there is no possibility for O_2 readsorption, due to the fact that its adsorption is inhibited by the adsorbed CO. The effect is intensified at higher temperatures because of higher oxygen desorption rates.

Summary of the simulation parameters

In summary, as introduced in the previous sections, our modeling framework for diffusion of gases in porous structure with surface adsorption and reaction requires 17 fitting parameters to define the process at a given temperature and pressure. In particular, in order to simulate the catalytic oxidation of CO over Pd NPs we need:

- the length of unit vector of the Pd surface crystal, a_0;
- two parameters for the LH reaction step, E_{LH} and ν_{LH};
- the maximum surface coverages of O and CO, $\theta_{max,O}$ and $\theta_{max,CO}$;
- two Kisluik adsorption parameters each for O_2 and CO, K and S_0;
- four parameters each for O_2 and CO to describe the desorption, namely E_{des}, W, C_a, and C_b.

Simulation Results and Discussion

Simulation geometry and procedure

In this section, we simulate the process of diffusion and catalytic reaction of CO and O_2 within Pd NP layers produced by

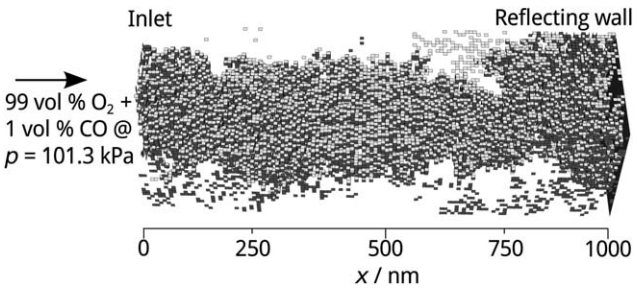

Figure 4. Porous layer with 8 nm cubes used for DSMC based simulation of gas diffusion and surface catalytic reactions.

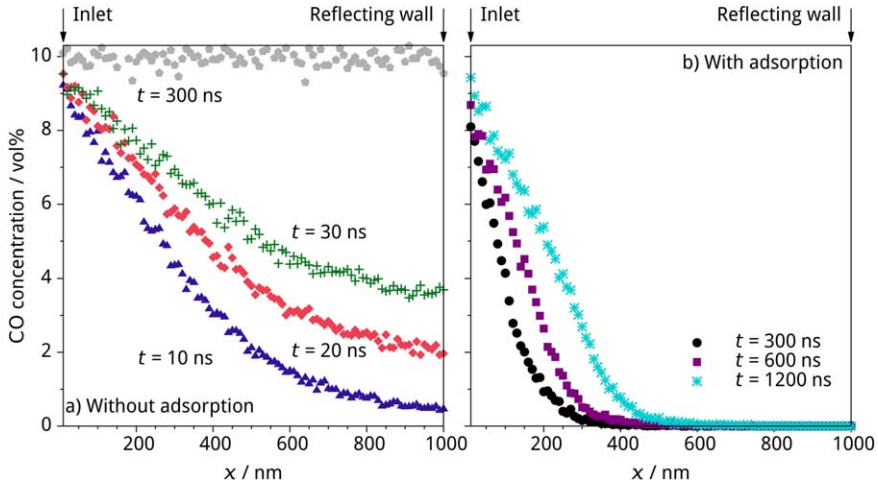

Figure 5. Local CO concentration during the diffusion of gas composed of 10 vol % CO and 90 vol % O_2 in a highly porous layer that was initially filled with oxygen at $p = 101.3$ kPa ($T = 323$ K).

The inlet was positioned at $x = 0$ and a reflecting wall at $x = 1000$ nm. (a) Diffusion without adsorption of CO on the NP surface and (b) diffusion with adsorption. [Color figure can be viewed in the online issue, which is available at wileyonlinelibrary.com.]

FSP. Both the layer structure and the (nonreactive) gas diffusion within it have been studied in previous works[13,17] using the DGM and DSMC. Without loss of generality, we assume that the particles expose only (111) surfaces, mainly because of the readily available data sets of the kinetic parameters for this system. The geometries of the layers are generated with raw data from Mädler et al.[17] Single mesh cells are cut from the positions of the individual NPs and replaced by solid cuboids with OpenFoam's mesh tool snappyHexMesh. In reality NPs often resemble spheres rather than cuboids. However, to reproduce spheres in the simulation, a highly irregular mesh with very small cells would have been necessary and would pose restrictions on the applicability of the binary collision model in DSMC.

An example of the resulting NP layers can be seen in Figure 4. The layers have a depth of $l = 1000$ nm, a quadratic cross section with edge lengths of 280 nm and a porosity ε of 92.6%. The NPs have an edge length of 8 nm, which results in a similar particle volume as spheres with 10 nm diameter. Porosity ε, pore area A, normalized differential pore area $\Delta A \cdot \left(\log\left[\Delta d_{\text{pore}}\right] \cdot \sum A\right)^{-1}$, and median pore diameter based on the Q_2 pore size distribution $d_{50,2}$ were calculated and compared with layers with full structure precision, viz. layers where the particles are represented by 10 nm diameter spheres.[13] The volume-based porosity of the layers with full precision is 93% which agrees well with the 92.6% of the simplified cuboid structures. Also, the $d_{50,2}$ pore sizes of both structures are very similar (58 nm for spheres and 60 nm for cuboids).

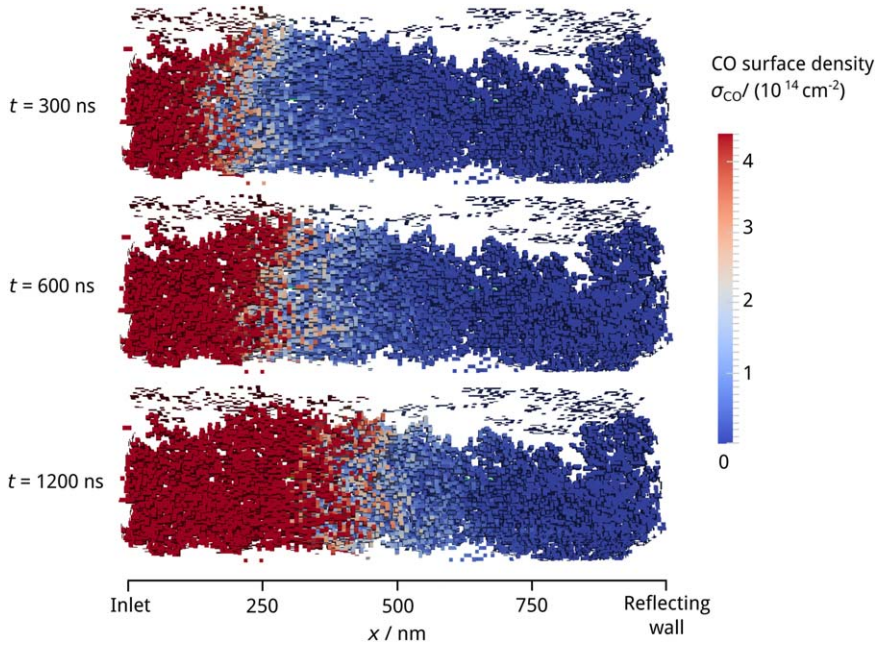

Figure 6. CO surface density σ_{CO} during the diffusion and adsorption of 10 vol % CO in a highly porous layer initially filled with oxygen ($p = 101.3$ kPa, $T = 323$ K).

[Color figure can be viewed in the online issue, which is available at wileyonlinelibrary.com.]

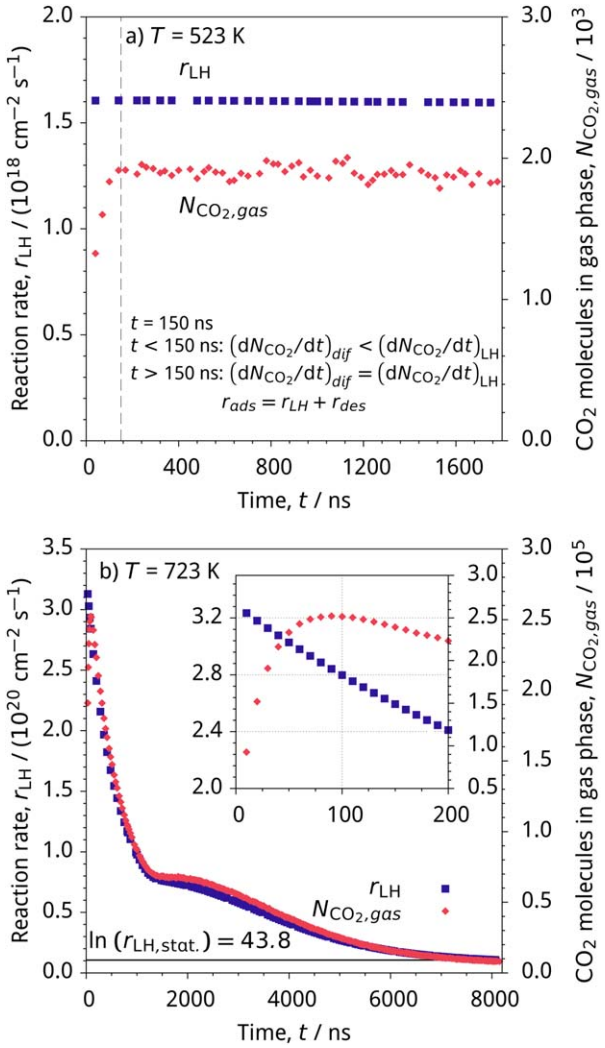

Figure 7. Reaction rate r_{LH} and amount of CO_2 molecules in the gas phase, $N_{CO_2,gas}$, as a function of time t during the CO oxidation of 1 vol % CO in 99 vol % O_2 at a pressure of $p = 101.3$ kPa for two different temperatures, $T = 523$ K (a) and $T = 723$ K (b).

The inset in (b) shows the first 200 ns in more detail. [Color figure can be viewed in the online issue, which is available at wileyonlinelibrary.com.]

The inlet was positioned at $x = 0$ nm and a reflecting wall representing the sensor substrate at $x = 1000$ nm. Cyclic boundary conditions were applied at the four longitudinal boundaries. The time step for simulation Δt was chosen to be 5×10^{-12} s, the amount of molecules per DSMC parcel F_N is 1, and the cell size $8\times8\times8$ nm^3 (so that each Pd NP fills an entire cell). The mean pore diameter of the layer yields a Kn number of about 1 for atmospheric conditions. Therefore, the gas diffusion model must be valid in the free molecular and slip flow regimes.

Diffusion of CO into porous layers

At first, we investigate the diffusion of 10 vol % CO in O_2 in the porous layers with and without adsorption at $T = 323$ K and $p = 101.3$ kPa. Initially, the NP surfaces are saturated with O_2, which at this low temperature does not appreciably desorb or resorb (see Figure 3). The obtained spatially resolved CO concentration profiles at different time steps are shown in Figure 5. Without adsorption (Figure 5a), a notable CO concentration reaches $x = 1000$ nm after 10 ns. With adsorption, however, even after 1200 ns, CO molecules only reach a layer depth of 500 nm (Figure 5b). As the surface density of CO is zero at $t = 0$, all of the initialized CO molecules adsorb on the NP surface during the first few wall contacts. This leads to a prolonged diffusion process as the particle surface acts as a sink for CO molecules. Diffusion into the layer is effectively occurring only after the surface becomes saturated with CO, as visible in Figure 6, where the CO surface densities for the three selected time steps are shown.

CO oxidation in porous layers

The catalytic CO oxidation in porous Pd(111) layers is simulated at different temperatures (from $T = 473$ K to $T = 823$ K) at $p = 101.3$ kPa and with a feed composition at the inlet of 1 vol % CO and 99 vol % O_2 (see Figure 4). Initially, the surface coverages of CO and O are set to the maximum coverages, $\sigma_{max,CO} = 4.06\times10^{14}$ molecules cm^{-2} and $\sigma_{max,O} = 3.34\times10^{14}$ molecules cm^{-2}, to start the simulation close to the expected steady state and to avoid latencies due to diffusion and adsorption of CO.

Figure 7 shows the reaction rate and the amount of CO_2 molecules in the gas phase as a function of time for $T = 523$ K (a) and $T = 723$ K (b). At $T = 523$ K, the reaction proceeds slowly and the surface coverage is constant with time. CO molecules entering the system through the inlet have sufficient time to diffuse through the layer and adsorb before the surface coverage decreases due the chemical reaction with O_2. In this case, a time-independent maximum surface coverage of CO and O is obtained, because the fluxes of both CO and O_2 through the layer are sufficient to replenish all consumed molecules. The amount of CO_2 gas phase molecules in the complete layer increases up to a steady-state value of approximately 1.9×10^3 molecules at $t > 150$ ns. At this point, the amount of accumulated CO_2 molecules in the layer due to the reaction is so high that the loss of CO_2 molecules through the inlet ($(dN_{CO_2}/dt)_{dif}$) matches the generation of molecules due to the reaction ($(dN_{CO_2}/dt)_{LH}$).

At $T = 723$ K the reaction is fast, while the flux of CO and O_2 molecules through the layer and the adsorption rate are insufficient to replenish all consumed molecules. This causes a shift of the adsorption–desorption–reaction equilibrium and the coverages of CO and O decrease with time. The proportionality of surface coverage and reaction rate leads to a monotonically decreasing reaction rate. Namely, the CO_2 concentration in the gas phase increases only for the first 100 ns (see inset), reaches a maximum and decreases afterwards. At $t = 8000$ ns the surface coverages and thus the reaction rate have decreased to an extent that diffusion and adsorption of the reactants match the consumption of molecules through the reaction. At this point the reaction rate hardly changes with time and we can safely assume, for our purpose, that the system has reached an overall steady state.

The local CO_2 concentration for different time periods as well as the CO and CO_2 concentrations at $t = 8000$ ns (steady state) are presented in Figure 8. As already mentioned, there is no generation of CO_2 molecules at the inlet. Therefore, the CO_2 concentration is lower close to the inlet (and almost 0 at $x = 0$) than at points at the far end of the layer (Figure 8, left). Additionally, the average concentration of CO_2 decreases with time, since the first data set is at $t = 150$ ns, which is already

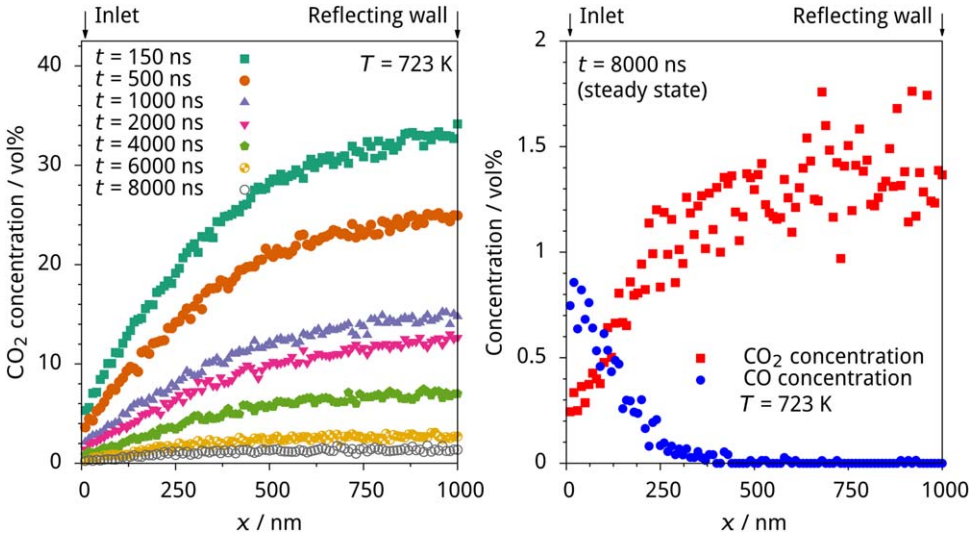

Figure 8. Local CO_2 concentrations taken at different times during the CO oxidation in a highly porous Pd layer of 1000 nm thickness with a reflecting wall at $x = 1000$ nm and an inlet at $x = 0$ ($T = 723$ K, $p = 101.3$ kPa and $p_{O_2}/p_{CO} = 0.99/0.01$).

At the beginning of the simulation, surface coverages of O_2 and CO were set to their maximum value. [Color figure can be viewed in the online issue, which is available at wileyonlinelibrary.com.]

after the peak-CO_2 concentration at $t = 100$ ns (N_{CO_2}, Figure 7b, inset, 723 K). The concentration profile at the steady state is shown in Figure 8 (right). The reaction is limited by mass transport and CO molecules entering the inlet only diffuse 250 nm into the layer, because of surface adsorption and reaction. At depths larger than 300 nm, the CO coverage in the reactor is zero, indicating that all initially adsorbed CO molecules have been consumed by the oxidation reaction.

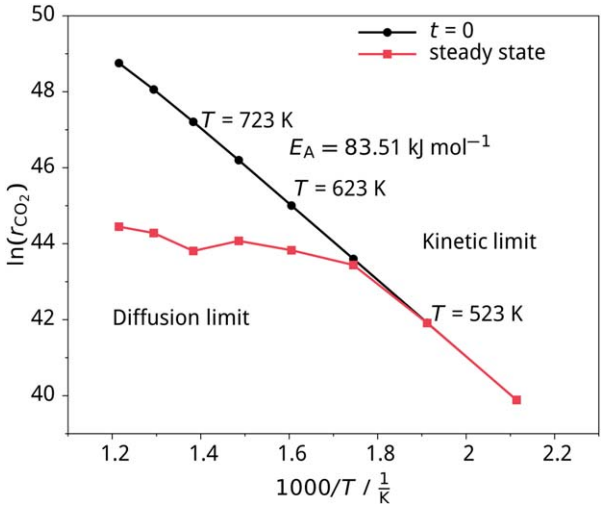

Figure 9. Arrhenius plot for the oxidation of 1 vol % CO in 99 vol % O_2 at a pressure of 101.3 kPa in a highly porous layer of 1000 nm thickness.

Initially, surface coverages of CO and O were set to maximum values, $\sigma_{max,CO} = 4.06 \times 10^{14}$ molecules cm^{-2} and $\sigma_{max,O} = 3.34 \times 10^{14}$ molecules cm^{-2}, respectively, resulting in a reaction rate at $t = 0$ represented by the straight black line. The slope of the reaction rate at $t = 0$ yields an activation energy of 83.51 kJ mol^{-1}, which matches exactly the activation energy of the LH step. The red line shows reaction rates at steady state for each respective temperature. [Color figure can be viewed in the online issue, which is available at wileyonlinelibrary.com.]

The results of the simulations at all investigated temperatures can be summarized in an Arrhenius plot linking the reaction rate of CO_2 generation with the reaction temperature either at the very beginning of the simulation ($t = 0$) or after reaching a steady state (e.g., after 8000 ns for $T = 723$ K) (Figure 9). All simulations were initiated with maximum surface coverages of O and CO. The corresponding reaction rates at $t = 0$ yield the activation energy of the LH step, which is the kinetic limit of the overall reaction. This value should be identical with the steady-state reaction rate of the system if both species have infinite diffusion coefficients and are added in a stoichiometric ratio. This is indeed the case for the lower temperatures investigated, where all CO and O molecules consumed in the (slow) reaction are replenished immediately by diffusion and adsorption. At temperatures higher than about 573 K, the surface reaction becomes faster than diffusion and adsorption, which thus become the rate limiting steps (diffusion limit).

We note in passing that at very high temperatures the reaction rate should increase again due to the gas-phase reaction between CO and O_2. This mechanism, however, is not currently taken into account in our algorithm implementation.

The transition between a reaction-limited to a diffusion-limited regime is also visible by looking at the profiles of the local normalized reaction rate η_x, that is, the local reaction rate divided by the maximum reaction rate found in the layer at a given temperature at steady-state conditions (Figure 10). For temperatures below 573 K, diffusive transport of reactants is faster than their reactive consumption, leading to a constant reactant coverage and a constant reaction rate, that is, $\eta_x = 1$ for all x. At $T = 673$ K or higher, two different effects occur. The region close to the inlet shows a lower reaction rate due to the poisoning by CO molecules, that is, the CO_{ads} surface density is very high and consequently the O_{ads} surface density is low, which is a result of the underlying adsorption model (see example in Figure 11b). In this region, the rate determining step of the overall process is thus the CO desorption. On the reflecting wall, η_x is smaller than 1 because O_{ads} dominates the surface. The CO concentration in the gas decreases

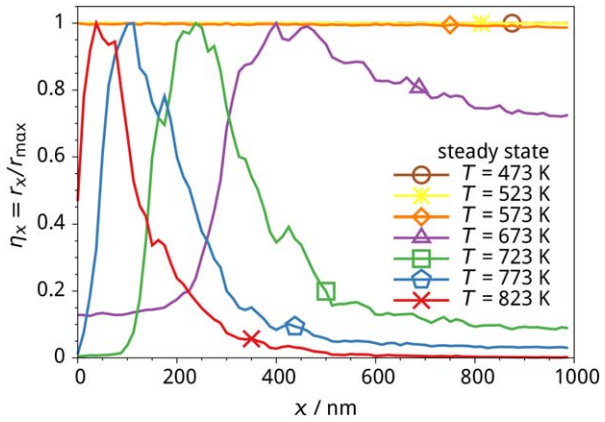

Figure 10. Local normalized reaction rate $\eta_x = r_x/r_{max}$ of the oxidation of 1 vol % CO in a highly porous nanoparticle layer of 1000 nm length filled with oxygen at $p = 101.3$ kPa.

[Color figure can be viewed in the online issue, which is available at wileyonlinelibrary.com.]

constantly with x due to the reaction, so that only an insufficient amount of CO molecules reach the far end of the NP layer. This leads to a low σ_{CO} in regions far from the inlet. The local normalized reaction rate η_x, as displayed in Figure 10, presents similarities to the well-known effectiveness factor η, which is a dimensionless number characterizing the (nonlocal) transition from mass-transport limitation to kinetic limitation of a reaction system. Here, in contrast, three interconnected phenomena occur, that is, diffusion limit, reaction limit, and reaction inhibition. We thus believe that the reaction rate η_x is better suited than the effectiveness factor η for describing the full transition of all sub-steps partaking in the overall reaction.

The unusual high degree of noise in the reaction rate displayed in Figure 10 is caused by the stochastic approach, which does not deliver continuous functions for the gas phase and surface concentrations. Additionally, resulting from the nature of the layer generation, the solid structure is inhomogeneously distributed along the depth of the layer. Thus, the surface per volume element of the layer is not constant along the leading dimension. These local fluctuations of active surface area vs. depth lead to the fluctuations in the reaction rate. An increased lateral dimension of the microstructure under investigation will lead to a smoother curve.

The interplay between mass-transport limitation, kinetic limitation and reactor poisoning can be better understood by looking at the time evolution of the local reaction rate at $T = 723$ K (Figure 11a). At early times ($t \leq 1000$ ns), the reaction rate (a) is highest at the inlet of the reactor, where adsorption of the incoming CO molecules and reaction with preadsorbed oxygen takes place. As time progresses, the O_{ads} surface coverage in the inlet region ($x < 125$ nm) decreases until complete depletion due to CO poisoning at the steady state (see the steady-state coverage profile of the two adsorbed species in Figure 11b). This also affects the reaction rate, due to the second-order dependence of r_{CO_2} (Eq. 14), which is zero if σ_O is zero. Because of the adsorption and reaction of CO molecules, the CO gas phase concentration at steady-state decreases from the inlet to $x = 300$ nm (cf. Figure 8, right) and accordingly also σ_{CO} decreases until it reaches zero at $x \approx 300$ nm. Inversely, as a consequence of the underlying adsorption model, σ_O increases until it reaches its maximum value of $\sigma_O \approx 3\times10^{14}$ cm^{-2} at $x \approx 300$ nm. Only in the crossover region between CO adsorption and O adsorption has the reaction rate a notable value, with its maximum exactly at the point where the coverage profiles intersect ($x \approx 250$ nm, stoichiometric conditions). The far end of the reactor is saturated with oxygen and does not participate in the reaction because CO does not reach this part before reacting to CO_2.

Discussions and Conclusions

The DSMC algorithm, implemented into the open source software package OpenFOAM, is a statistical approach to model gas diffusion and convection in the transition regime based on direct calculation of tracks and collisions of single molecules, applicable over a wide range of scales. We have now extended this algorithm to model gas-solid catalytic

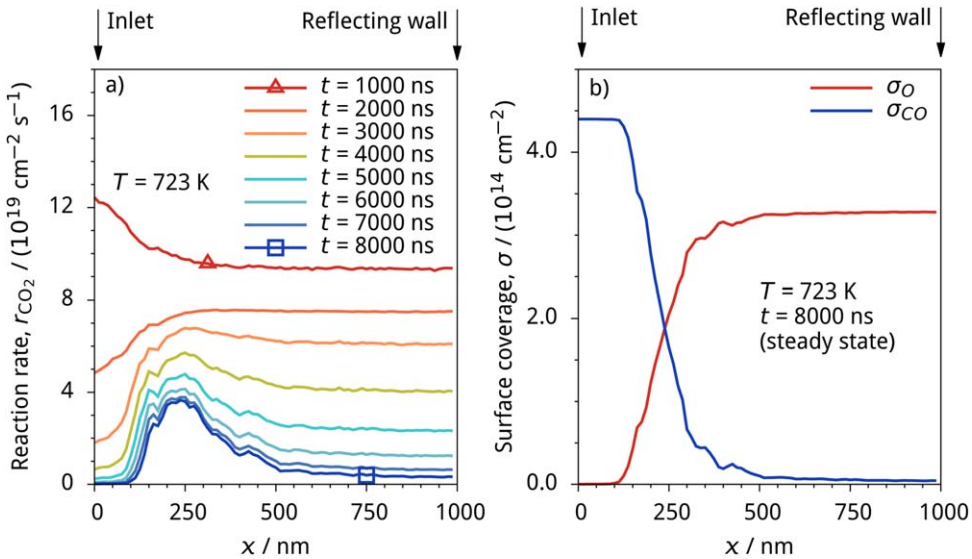

Figure 11. a) local reaction rate r_{CO_2} and b) CO and O surface densities, σ_{CO} and σ_O, respectively, at $t = 8000$ ns (1 vol % CO at $p = 101.3$ kPa and $T = 723$ K).

[Color figure can be viewed in the online issue, which is available at wileyonlinelibrary.com.]

reactions, using a local mean field approximation to treat individual chemical processes occurring at the gas/solid interface. Namely (1) molecular adsorption is modeled through sticking coefficients calculated by means of the precursor-mediated Kisluik approach; (2) desorption of molecules is based on the Polanyi-Wigner equation; (3) reactions between adsorbed molecules are modeled through an Arrhenius equation based on surface coverages. The presented algorithm thus link the microscale (surface chemical processes) with the mesoscale (diffusion inside porous structures), and could also include macroscale transport processes by the employment of the DSMC parcel concept.[10] It offers the possibility of simulating catalytic or sensing processes within a reasonable time compared with more elaborate approaches such as MD.

In general, MC methods are well suited to study grand-canonical systems because the insertions and deletions of particles are easily performed during the stochastic movements. However, in order to preserve thermodynamic consistency, the state variables have to satisfy the four laws of thermodynamics, that is, the model has to deliver consistent enthalpy diagrams as well as consistent entropy changes in the overall reaction. A method to develop microkinetic models which fulfill thermodynamic consistency is given by Dumesic et al.[34] or in a slightly modified form, by Salciccioli et al.[9] In the case of the simulations shown here, consistency within the microkinetic framework of our investigation (gas transport and reaction kinetics) is achieved by fits of all simulation parameters to actual surface science experiments. However, it does not guarantee thermodynamically consistent statistics because it is not based on the conservation of an appropriate thermodynamical potential. In future work, this may be realized by the implementation of heat-exchange models to take into account the cross-correlated enthalpy and entropy changes associated to each individual process step. Such heat exchange models could for example include the temperature increase of the solid material due to the exothermic reaction and a transfer of energy from the NPs to the gas molecules and vice versa.

In this article, we have applied our newly developed model to study the catalytic oxidation of CO in porous Pd NP layers, thus extending previous work devoted to the diffusion of CO inside these layers.[13] We have identified steady states between gas diffusion of reactants (CO and O_2) and products (CO_2), adsorption/desorption of the reactants, and chemical reaction at the surface with formation of the products for different temperature regimes. In particular, at temperatures below about 573 K the reaction is governed by a kinetic limit, where gas diffusion and adsorption is fast and the surface chemical reaction step is rate determining. At temperatures above 573 K the reaction is limited by mass transport, since diffusion and adsorption are slow compared with the catalytic reaction, which results in a regime in which the reaction rate is nearly constant with temperature, albeit the reaction-rate equation contains an exponential temperature dependence.

The method also allows the precise evaluation of local reaction rates over the depth of the reactor. We have shown that the reactor becomes poisoned by CO at high temperatures in an area close to the inlet, since adsorbed CO_{ads} hinders oxygen adsorption. Behind the poisoned area, the inverse variation of the CO_{ads} and O_{ads} coverages results in a peak of the reaction rate in the specific reactor region where the coverage profiles intersect. At areas close the end of the reactor, the O_{ads} coverage is high but the CO_{ads} coverage is low due to previous consumption of the incoming CO, again resulting in a low overall reaction rate. This kind of analysis allows an optimization of the reactor structure to optimize the catalytic (or sensing) performance while reducing the overall system size and thus the associated fabrication costs.

Although the presented results demonstrate the functional capabilities of the developed simulation algorithm, we would like to stress that our parameter set is not strictly relevant to the study of the real CO oxidation catalysis, being taken from experiments at very low gas pressure and used under conditions close to atmospheric pressures. Moreover, the simulation system itself neglects surface-diffusion processes and uses the mean field approximation for the kinetic modeling. The latter may be a rather poor assumption for catalytic reactions,[35] especially for the case of dissociatively adsorbing O_2 coupled with reactions that consume only one of the two O atoms. This may lead to unavoidable fluctuations in composition, for example, the local number of nearest neighbors of a specific species may not be equal to the mean number of neighbors. Additionally, in reaction systems in which repelling interactions between unlike molecules is higher than the interaction energy between like molecules, domain formation occurs, which is also the case for CO oxidation over Pd(111). However, this island formation can be modeled correctly only if molecules have distinct positions on the surface and are able to surface-diffuse, as it is the case for instance in explicit kMC simulations.[36] A correct modeling of domain formation might not be necessary if simulations are only examining reactions in small temperature and (partial-) pressure windows, in which the simulation parameters do not change much due to segregation. Most of the reaction parameters were taken from different literature sources and simulations were conducted under different reaction conditions compared with the experiments. Additionally, the parameters were taken from well-defined single crystal surfaces and thus do not represent real reaction systems. This makes a comparison of our simulations with experimental data difficult. In future studies, we plan to extract all parameters from one real reaction system, which would allow for a quantitative comparison of simulations with experimental results. Real reaction systems show surface defects, which, in general, display lower adsorption and reaction barriers compared with the bulk barriers on well-defined surfaces. In addition, the reaction barrier on Pd at atmospheric pressure is much lower than the UHV barrier used in this study. As a consequence, the presented algorithm is expected to underestimate the experimental reaction rate.

A comparison of the presented results with well-known theories, such as the reaction–diffusion equation with a LH reaction term, fails because of the different approach of our algorithm. In such theories, an equilibrium of adsorption and desorption is established faster than the reaction proceeds and the rate-determining step (RDS) of the surface processes is the reaction step itself. In addition, those theories may include competitive adsorption, but do not include a complete modeling of the surface processes and thus do not include inhibition by one of the reactants. For comparison, it would be necessary to establish a reaction term which includes all surface chemical processes, that is, adsorption (including the influence of adsorbed CO on oxygen adsorption), desorption, and reaction. It would then be necessary to find the RDS of these processes, which might change with temperature and position in the layer. For instance, at low temperatures, the rate-determining step would be the reaction step. At high temperatures, the RDS is the CO desorption at positions close to the inlet, the

reaction at positions in the center of the reactor, and the diffusion at positions close to the wall. The establishment of such a model is beyond the scope of this work.

Acknowledgments

The author would like to thank Jochen Dreyer from the City University of Hong Kong for discussion. GP would like to thank the German Research Foundation (DFG) for financial support through the research training group "Micro-, meso-, and macroporous nonmetallic Materials: Fundamentals and Applications" (GRK 1860) and Lars Kiewidt (UFT, University of Bremen) for helpful discussion regarding the modeling of chemical reactions. LM and LCC thank the DFG for funding within the priority program "Partikel im Kontakt – Mikromechanik, Mikroprozessdynamik und Partikelkollektive" (SPP 1486) under grants MA 3333/3 and CO 1043/3.

Literature Cited

1. Keil FJ. Modeling reactions in porous media. In: Deutschmann O, editor. *Modeling and Simulation of Heterogeneous Catalytic Reactions: From the Molecular Process to the Technical System*, Chap. 5, Weinheim, Germany: Wiley-VCH. 2012: 149–186.
2. Deutschmann O, editor. *Modeling and Simulation of Heterogeneous Catalytic Reactions: From the Molecular Process to the Technical System*. Weinheim: Wiley-VCH, 2012.
3. Parr RG, Yang W. *Density Functional Theory of Atoms and Molecules*. New York: Oxford University Press. 1989.
4. Jansen APJ. *An Introduction to Monte Carlo Simulations of Surface Reactions*. Heidelberg: Springer, 2012.
5. Mason EA, Malinauskas AP. *Gas Transport in Porous Media: The Dusty-Gas Model*. Amsterdam: Elsevier, 1983.
6. Janardhanan VM, Deutschmann O. CFD analysis of a solid oxide fuel cell with internal reforming: coupled interactions of transport, heterogeneous catalysis and electrochemical processes. *J Power Sources*. 2006;162:1192–1202.
7. Votsmeier M. Efficient implementation of detailed surface chemistry into reactor models using mapped rate data. *Chem Eng Sci*. 2009;64: 1384–1389.
8. Reuter K, Stampfl C, Scheffler M. Ab initio atomistic thermodynamics and statistical mechanics of surface properties and functions. In: Yip S, editor. *Handbook of Materials Modeling*. Dordrecht, Netherlands: Springer, 2005, 149–194.
9. Salciccioli M, Stamatakis M, Caratzoulas S, Vlachos DG. A review of multiscale modeling of metal-catalyzed reactions: mechanism development for complexity and emergent behavior. *Chem Eng Sci*. 2011;66:4319–4355.
10. Bird GA. Molecular Gas Dynamics and the Direct Simulation of Gas Flows. New York: Oxford University Press, 1994.
11. Bird GA. Chemical reactions in DSMC. AIP Conf Proc. 2011;1333: 1195–1202.
12. Scanlon TJ, Roohi E, White C, Darbandi M, Reese JM. An open source, parallel DSMC code for rarefied gas flows in arbitrary geometries. *Comput Fluids*. 2010;39:2078–2089.
13. Dreyer JAH, Riefler N, Pesch GR, Karamehmedovic M, Fritsching U, Teoh WY, Mädler L. Simulation of Gas Diffusion in Highly Porous Nanostructures by Direct Simulation Monte Carlo. *Chem Eng Sci*. 2014;105:69–76.
14. Mädler L, Roessler A, Pratsinis SE, Sahm T, Gurlo A, Barsan N. Direct formation of highly porous gas-sensing films by in situ thermophoretic deposition of flame-made $Pt/Sn/O_2$ nanoparticles. *Sens Actuat B: Chem*. 2006;114:283–295.
15. Großmann K, Kovács KE, Pham DK, Mädler L, Barsan N, Weimar U. Enhancing performance of FSP SnO_2-based gas sensors through Sb-doping and Pd-functionalization. *Sens Actuat B: Chem*. 2011;158:388–392.
16. Sahm T, Mädler L, Gurlo A, Barsan N, Pratsinis S, Weimar U. Flame spray synthesis of tin dioxide nanoparticles for gas sensing. *Sens Actuat B: Chem*. 2004;98:3764–3772.
17. Mädler L, Lall AA, Friedlander SK. One-step aerosol synthesis of nanoparticle agglomerate films: simulation of film porosity and thickness. *Nanotechnology*. 2006;17:4783–4795.
18. Engel T, Ertl G. Elementary steps in the catalytic oxidation of carbon monoxide on platinum metals. *Adv Catal*. 1979;28:1–78.
19. McClure SM, Goodman DW. New insights into catalytic CO oxidation on Pt-group metals at elevated pressures. *Chem Phys Lett*. 2009;469:1–13.
20. Kolasinski KW. Surface Science. The Foundation of Catalysis and Nanoscience, 3rd ed. Chichester: Wiley, 2012.
21. Guo X, Yates JT. Dependence of effective desorption kinetic parameters on surface coverage and adsorption temperature: CO on Pd(111). *J Chem Phys*. 1989;90:6761–6766.
22. Gentle JE. Random Number Generation and Monte Carlo Methods. New York: Springer, 2003.
23. Somorjai GA, Li Y. Introduction to surface chemistry and catalysis, 2nd ed. Hoboken: Wiley, 2010.
24. Kisluik P. The sticking probabilities of gases chemisorbed on the surfaces of solids. *J Phys Chem Solids*. 1957;3:95–101.
25. Kisluik P. The sticking probabilities of gases chemisorbed on the surfaces of solids—II. *J Phys Chem Solids*. 1958;5:78–84.
26. Gong XQ, Raval R, Hu P. General insight into CO oxidation: a density functional theory study of the reaction mechanism on platinum oxides. *Phys Rev Lett*. 2004;93:106104.
27. Engel T, Ertl G. A molecular beam investigation of the catalytic oxidation of CO on Pd(111). *J Chem Phys*. 1978;69:1267–1281.
28. Conrad H, Ertl G, Küppers J, Latta EE. Interaction of NO and O2 with Pd(111) surfaces. *Surf Sci*. 1977;65:235–244.
29. Conrad H, Ertl G, Küppers J, Latta EE. Interaction of NO and O2 with Pd(111) surfaces. II. *Surf Sci*. 1977;65:245–260.
30. Leisenberger FP, Koller G, Sock M, Surnev S, Ramsey MG, Netzer FP, Klötzer B, Hayek K. Surface and subsurface oxygen on Pd(111). *Surf Sci*. 2000;445:380–393.
31. de Jong AM, Niemantsverdriet JW. Thermal desorption analysis: comparative test of ten commonly applied procedures. *Surf Sci*. 1990;233:355–365.
32. Guo X, Hoffman A, Yates JT. Adsorption kinetics and isotopic equilibration of oxygen adsorbed on the Pd(111) surface. *J Chem Phys*. 1989;90:5787–5792.
33. Creighton JR, Tseng FH, White JM, Turner JS. Numerical modeling of steady-state carbon monoxide oxidation on Pt and Pd. *J Phys Chem*. 1981;85:703–708.
34. Dumesic JA, Huber GW, Boudart M. Rates of catalytic reactions. In: Ertl G, Knözinger H, Schüth F, Weitkamp J, editors. *Handbook of Heterogeneous Catalysis*. Wiley-VCH, 2008:1445–1462.
35. Temel B, Meskine H, Reuter K, Scheffler M, Metiu H. Does phenomenological kinetics provide an adequate description of heterogeneous catalytic reactions? *J Chem Phys*. 2007;126:204711.
36. Farkas A, Hess F, Over H. Experiment-based kinetic Monte Carlo simulations: CO oxidation over $RuO_2(110)$. *J Phys Chem C*. 2012; 116:581–591.

Manuscript received Nov. 3, 2014, and revision received Mar. 17, 2015.